Work function investigations of Al-doped ZnO for band-alignment in electronic and optoelectronic applications

Grant Drewelow[b], Austin Reed[b], Chandon Stone[b], Kwangdong Roh[c], Zhong-Tao Jiang[d], Linh Nguyen Thi Truc[e], Kwangsoo No[f], Hongsik Park[g], Sunghwan Lee[a,b,*]

[a] School of Engineering Technology, Purdue University, West Lafayette, IN 47907, USA
[b] Department of Mechanical Engineering, Baylor University, Waco, TX 76798, USA
[c] Department of Electrical Engineering, Princeton University, Princeton, NJ 08544, USA
[d] School of Engineering and Information Technology, Murdoch University, Murdoch, WA 6150, Australia
[e] Department of Chemistry, Ho Chi Minh City University of Education, Ho Chi Minh City 70250, Vietnam
[f] Korea Advanced Institute of Science and Technology, Department of Materials Science and Engineering, Daejeon 34141, South Korea
[g] School of Electronics Engineering, Kyungpook National University, Daegu 702-701, South Korea

Keywords: ZnO; Al-doped ZnO (AZO); Work function; Fermi energy level; Band alignment; X-ray photoelectron spectroscopy

*Corresponding authors: sunghlee@purdue.edu

Abstract

Possessing the ability to tune the work function and band gap of transparent conducting oxides (TCOs) is widely sought after, as it allows for improved band alignment in electronic and optoelectronic applications, enhancing overall device performance. Out of the many TCOs, Al-doped zinc oxide (AZO) has received considerable interest for electrode application due to its low electrical resistivity, high optical transparency in the visible regime, and room-temperature fabrication capability. In this study, we report on the effects of post fabrication air-annealing on the work function and band alignment of AZO deposited at room temperature by DC-magnetron sputtering. AZO films were air-annealed at temperatures varying from 25 °C (as-deposited) to 600 °C. The Fermi energy levels, work function values, surface chemistry, and optical band gaps of the AZO films were investigated via X-ray photoelectron spectroscopy (XPS) and UV-Vis spectroscopy. An increase of the work function from ~5.53 eV to ~6.05 eV is observed to take place over an increase of annealing temperatures from 25 °C (as-deposited) to 600 °C, determined to be the result of a decrease in carrier concentration through the promoted extinction of oxygen vacancies. Via XPS analysis, the increased extinction of oxygen vacancies was confirmed due to a notable shift from an oxygen-deficient state to an oxygen-sufficient state in the high resolution O 1s peaks, for which the activation energy was found to be 33.3 meV. Over the course of increasing annealing temperatures, the optical band gap saw a shift from ~3.55 eV to ~3.37 eV, following the Burstein-Moss phenomenon due to a decrease in carrier concentration, further verifying an increase in oxygen vacancy extinction. The reported results confirm that work function tuning of AZO films can be achieved through simple post-fabrication air-annealing.

1. Introduction

Transparent conducting oxides (TCOs) belong to a unique class of materials which combines characteristically high transparency in the visible regime with high electrical conductivity. This particular set of properties makes TCOs essential in the development of new technologies which require high-performance optoelectronic capabilities such as, but not limited to, ultra-high-resolution displays [1-3] , light-emitting diodes [4, 5], flexible electronics [2, 4], and front-surface electrodes for solar cells [1, 6]. As the rate of technological advancement in the field of electronic devices continues to grow, the demand for novel TCOs which meet the needs of the desired applications correspondingly increases. Thus, it is imperative to continue investigating, synthesizing, and modifying TCO materials in order to find the optimal TCO for each respective application.

Out of the many TCO materials, Zinc Oxide-based (ZnO) thin films show significant promise, exhibiting extraordinary potential due to their low-cost and abundant raw material [6], non-toxic nature [6, 7], excellent thermal stability [6], and highly transparent properties in the visible regime [8, 9]. While pure ZnO films exhibit low and unstable electrical conductivities, prior research has shown that the group III impurity doping (Ba [10, 11], Al [12, 13], Ga [11, 14], In [11, 15]) of ZnO allows for ZnO-based TCOs to achieve high electrical conductivities whilst maintaining their high levels of transparency. Among the many impurity-doped ZnO films, Al-doped ZnO (AZO) exhibits the lowest electrical resistivity of ~2-4 x 10^{-4} Ω-cm at an Al_2O_3 content of 1-2 wt. % [12, 16, 17], identifying AZO as the outstanding impurity-doped ZnO-based TCO. Furthermore, AZO exhibits the capability to be fabricated at low temperature conditions (RT-200 °C)[18, 19], a necessary requirement when developing electronic devices on temperature-sensitive materials.

Due to the unique combination of these promising characteristics, AZO is currently being investigated as a major TCO candidate in a variety of electronic applications such as thin film transistors (TFTs) [20, 21], thin film solar cells [22, 23], and organic electronic devices [5, 24].

In device applications which fundamentally rely on charge transfer between the channel/active layer and electrode materials (such as solar cells), preferred interfacial contact characteristics are sought to be Ohmic and low in resistivity [25, 26]. Ohmic contact at the heterojunction interface must be achieved as it ensures that undesirable charge obstruction is mitigated, allowing for sufficient charge transport between layers. However, inadequate contact between the two layers may occur due to the mismatching of electrode and active layer work function values [27, 28] along with the formation of interfacial dipoles [27, 29] and trap states [27, 30]. In order to address the adverse effects of mismatched work functions, numerous techniques which focus on electrode work function tuning such as, but not limited to, self-assembled monolayer treatments [31] and chemical modification [32, 33], have emerged as viable approaches for improving interfacial Ohmic contact characteristics.

In recent years, several attempts have been made to effectively tune the work function values of AZO in order to expand its breadth of application [16, 34]. In 2003, Jiang et al. discovered that the work function of AZO is dependent on the concentration of Al-dopant in the material, with a distinct variation in work function values from 3.7 eV to 4.4 eV at Al at. % ranging from 0.7 to 2.1, respectively [16]. However, altering wt. % of Al-dopant material has a significant effect on the thermal stability and optoelectronic properties of AZO [12, 16], thus limiting the viability of work function tuning through Al wt. % variation. More recently, Feng *et al.* [35] and Wang et al.

[34] further investigated AZO work function tuning through acetone solvent cleaning, during-deposition substrate-temperature variation (250-350 °C), and UV-ozone post-treatment exposure (as well as verifying the effects of Al-doping concentration). UV-ozone exposure was found to increase work function values by a maximum of ~0.4 eV at exposure times ≥ 20 minutes [34, 35], where substrate-temperature variation was shown to have no significant effect on AZO work function values in the observed temperature range [16]. Acetone solvent cleaning of the AZO films demonstrated a slight increase of in work function (~0.1 eV), yet proved to be inferior to the effects of UV-ozone post-treatment [34]. In both studies, it was concluded that these positive shifts in work function due to surface cleaning methods were primarily due to two factors: (i) a decrease in carbon contamination and (ii) an increase in the stoichiometric ratio of AZO, $[O_{ZnAl}]/([Zn]+1.5[Al])$ [34, 35]. Though a decent amount of AZO work function tuning procedures have been explored, there still may remain a number of tuning techniques which have yet to be discovered and, thus, it is important to continue investigating AZO work function tuning methods through novel and innovative approaches.

In this study, a simple and straightforward work function tuning technique for AZO is revealed through the process of post-fabrication air annealing. As it has been shown that oxygen vacancies are one of the primary carrier doping mechanisms in AZO [36], basic air annealing is conceived to be a viable method for controlling the overall carrier density of the thin film material. In the case of AZO, an n-type degenerated semiconductor, the Fermi level, and subsequently the work function, is expected to shift with a change in carrier concentration [37]. Therefore, post-fabrication air annealing should prove to be a simple yet effective technique which can be used to control the work function of AZO. In this paper, we report on the work function and band gap

tuning of AZO thin films fabricated via DC-magnetron sputtering through post fabrication air-annealing. The effects of post fabrication air-annealing on AZO's band characteristics, microstructural/chemical composition, and optoelectronic properties, are discussed in full detail.

2. Experimental

AZO films were prepared via DC-magnetron sputtering utilizing a sintered 2 wt.% Al_2O_3-doped ZnO target. Before sputtering took place, the deposition chamber was pumped down to a base pressure of $<5x10^{-6}$ Torr in order to eliminate the presence of foreign contaminants in the sputter gases. Once adequate vacuum level was achieved, Ar was introduced to the chamber in order to maintain a working pressure of $\sim 4x10^{-3}$ Torr. Base and working pressures were monitored throughout the deposition process via cold-cathode and pirani gauges, respectively. Substrate temperature was held constant at 25 °C (room temperature) and films were deposited onto both glass and Si substrates at a target-substrate distance of 10 cm. The substrates were rotated at a constant 10 rpm throughout the fabrication process to ensure film uniformity. In order to secure consistency in the analysis of the AZO films, all films were fabricated at a thickness of approximately 200 nm, which was measured using an FS1 multi-wavelength ellipsometer (Film Sense).

X-ray photoelectron spectroscopy (XPS) was implemented to determine the chemical compositions, chemical bonding, work function values, and valence states of both as-deposited and air-annealed AZO thin films. XPS analysis was performed using a Thermo Scientific K-Alpha XPS spectrometer under high vacuum ($<2x10^{-8}$ Torr) with focused monochromatic Al Kα X-ray radiation at 1486.7 eV and an electron flood gun in order to prevent charging of the thin films.

Photoelectrons were collected at an angle of 55° from the surface normal. For work function measurements, the samples were biased negatively in respect to the earth (V_{bias} = -30 V) in order to accelerate the emitted electrons and detect the onset of emission. Before work function data was collected, a gold specimen was used as reference in order to calibrate the spectrometer and the binding energy scale, allowing for accurate determinations of both the onset energy and fermi level position. The work function of the gold was measured to be 5.1 eV, in good agreement with the reported value [38], validating the reliability of the work function measurements in hand.

Crystallinity, orientation, and composition were investigated via x-ray diffraction (XRD) utilizing a Rigaku D/MAX-RC diffractometer by means of Cu Kα radiation (λ=1.54 Å) set at 40 kV and 40 mA. All samples were scanned continuously in a θ-2θ coupled scan at diffraction angles (2θ) ranging from 25° to 75°. The surface morphology and microstructure of as-deposited and annealed films were analyzed using a Philips XL30SFEG scanning electron microscope (SEM). Atomic force microscopy (AFM, Veeco Multimode) was employed to complement SEM surface investigations and to measure root mean square (RMS) roughness of the AZO surfaces in a non-contact height mode.

Both the transmittance and absorbance data of the AZO films in the 200-1000 nm wavelength spectra were gathered using a UV-Vis spectrometer (UV-3101PC, Shimadzu).

3. Results and discussion

In this study, XRD and SEM measurements were employed in order to investigate the effects of post-fabrication air-annealing on AZO film crystallinity and microstructure. Figure 1(a) shows

XRD patterns of air-annealed AZO at varying temperatures of 25 °C (as-deposited), 150 °C, 300 °C, 450 °C and 600 °C. XRD pattern analysis reveals that all AZO films investigated are in the crystalline state with preferred orientations located in the (002) crystallographic plane at a 2θ value of ~34.4°. This preferred orientation is the characteristic peak of hexagonal wurtzite ZnO [39]. Figures 1(b) and 1(c) display the microstructural effects of air-annealing AZO via SEM plan and cross-sectional images of as-deposited and 600 °C-annealed films, respectively. Notable grain boundaries are clearly observed in both SEM images, coinciding with the crystalline structures represented via XRD analysis. In regard to crystallite size, the as-deposited grains are shown to be approximately ~40 nm in diameter when measured via plan SEM imaging, growing to grain sizes of ~100 nm when introduced to air-annealing at 600 °C. The same effect can also be observed in the cross-sectional images of Figures 1(b) and 1(c), where the height variation on the surface is more prominent in the 600 °C-annealed sample than that of the as-deposited film due to the larger average grain size of the annealed films. The increased grain sizes of the annealed AZO films can be explained through the phenomena of annealing-induced small grain coalescence via grain boundary diffusion [40, 41], resulting in a larger average grain size while in strong agreement with other annealed-AZO and -ZnO studies.

Figure 2 provides further insight into the microstructural effects of air-annealing AZO, displaying changes in surface topography and RMS roughness due to increased annealing temperatures. Via non-contact mode AFM analysis, it can clearly be seen that the RMS roughness of AZO increases along with air-annealing temperature. While roughness values do increase from 25 °C (as-deposited) to 300 °C, the surfaces appear to remain relatively smooth throughout the annealing process with roughness values remaining below 3nm. When annealed at temperatures >450 °C, the

films exhibit a substantial increase in roughness, 5.12nm at 450 °C and 5.71nm at 600 °C, which is attributed to enhanced crystallinity and a sharp increase in grain size/coarseness. The microstructural effects observed in the annealed AZO samples are in good agreement with prior AZO research, where increased annealing temperature has been shown to directly relate to increased roughness and crystallinity [40, 42]. Furthermore, the topographical images obtained via AFM in Figure 2 are further verified via the previous XRD and SEM analyses, which also display an increase in crystalline structure in response to enhanced annealing temperatures.

In Figure 3, the effects of post-fabrication annealing on AZO's valence band (VB) spectra in relation to the Fermi energy level are represented via XPS analysis. In Figure 3(a), the peaks located at ~5 eV are said to be attributed to the involvement of both O 2p orbitals and hybridized O 2p/Zn 4s orbitals, whereas the peaks located around ~11 eV are indicative of the Zn 3d band [43]. The box figure located in Figure 3(a) can be seen more clearly in 3(b), which exhibits a clear shift in both the intensities and the binding energy locations of the hybridized O 2p peaks due to the variations in annealing temperature. Once the curves displayed in Figure 3(b) are linearly fitted, the straight-line intersection points with the baseline indicate the onset of photoexcitation, which gives the VB energy level, E_V, in relation to the Fermi energy level, E_F (E_F is simply located at 0 eV since the E_F of the sample and spectrometer are equalized.)[44-46]. Figure 3(c) displays the direct relationship between the VB's proximity to E_F, defined as E_F-E_V, and the temperature at which the AZO samples were annealed. As can be observed, a clear negative Fermi shift occurs due to increased air-annealing temperatures, with a maximum shift of ~0.4 eV occurring at 600 °C. Since AZO is known to possess n-type conduction properties, a Fermi shift towards the valence band indicates a decrease in carrier density due to an increase in annealing temperature. In order

to further understand why annealing temperature plays an important role in altering the carrier density of AZO films, the fundamental carrier mechanisms of AZO must first be established. Generally, there are two primary mechanisms which control carrier density in AZO thin films: (i) the generation of zinc interstitial atoms and (ii) the formation of oxygen vacancies [36]. However, two aspects of this particular study eliminate the possibility of changes in Zn content in the films: (i) AZO films were fabricated using a single, hot-sintered AZO target and (ii) annealing processes were completed using identical samples. Therefore, any changes in carrier concentration of these AZO films can be attributed solely to the formation (increase) or extinction (decrease) of oxygen vacancies. As electrical conductivity is directly dependent on the carrier concentration of the material, the total amount of oxygen vacancies can be said to play a significant role in overall thin film performance [47]. The doping mechanisms in AZO associated with oxygen-vacancies can be defined by[48, 49]:

$$O_o^x = \frac{1}{2} O_{2(g)} + V_{\ddot{O}} + 2e^- \quad (1)$$

where O_o^x denotes an oxygen atom on the oxygen sub-lattice and $V_{\ddot{O}}$ is a doubly-charged oxygen-vacancy which liberates two free electrons, effectively doping the carrier concentration of n-type AZO. Thus, increasing the annealing temperature in ambient air conditions promotes the extinction of carriers through filling oxygen vacancies with the oxygen content available in the air, subsequently decreasing overall carrier density and shifting the Fermi energy level closer to the VB. The carrier density of the AZO films were characterized through Hall Effect measurements in the van der Pauw configuration and the results are shown in Figure S1. The carrier density trend as a function of annealing temperature in Figure S1 is well matched with the results of E_F as well as work function and XPS elemental measurements that are discussed later in more detail. These measurements of E_F, work function, XPS elemental scans and Hall Effect support the discussion

that the oxygen vacancy-based doping/dedoping mechanism governs the change in carrier density of AZO in the present study.

For the effect of surface roughness on XPS measurements, it has been reported that the surface roughness may produce a lowering of XPS signals that is of particular relevance to depth profiling for elemental concentration analysis as a function of distance from the surface of samples[45, 50]. It also have been reported that although the surface roughness may affect the XPS intensity, the electron photo excitation energy is independent of the surface roughness[50]. Further, Gunter and Niemanstsverdriet *et al.*[51] reported that the surface planarity within the deviation less than 10 nm yields no significant reduction in the XPS intensity because the XPS technique typically probes upper ~20-30 nm of specimens. In the present study, the AZO thin films with a thickness of 200 nm show changes in roughness less than 4 nm as a function of annealing temperature. In addition, the determination of the Fermi energy level through the measurements is mainly governed by the photoexcitation energy (i.e., the location of onset binding energy) rather than the intensity. Therefore, the effect of the surface roughness on the investigation of the Fermi level is very minor or negligible in this study.

In order to determine the effects of post-fabrication air-annealing temperature on the work function of AZO, XPS analysis was performed on all AZO samples (as-deposited and annealed) in order to determine both the secondary electron cut-off (SECO) and high-energy cut off (HECO) points of the films. Basic principles of electron spectroscopy [52] allow for the calculation of the work function through the equation shown below:

$$\Phi = h\upsilon - \Delta E \tag{2}$$

where Φ is the work function of the material in eV, hv is the excitation energy at which the XPS measurements were gathered (1486.7 eV), and ΔE is defined by the difference of the HECO and SECO kinetic energies. Figures 4(a) and 4(b) display the SECO and HECO points, respectively, of the as-deposited AZO film. In order to determine the energy defined by the SECO point, a fit was applied to the linear regime of the curve with a baseline intersection point resulting in a SECO kinetic energy of 32.03 eV for the as-deposited film. Figure 4(b) displays the HECO point for the as-deposited specimen, located at ~1513.20 eV. With the SECO/HECO analyses executed in conjunction with Equation (2), the work function of the as-deposited film was determined to be ~5.53 eV. This process was then performed for all AZO samples under current study, allowing for the comparison of AZO's work function in respect to post-fabrication air-annealing temperature. In Figure 4(c), the overall dependency of AZO's work function on annealing temperature is displayed, where it can be clearly seen that an increase in work function from ~5.53 eV to ~6.05 eV occurs over an increase of annealing temperature from 25 °C (as-deposited) to 600 °C. Since the work function of a material is defined as the required energy to remove an electron from E_F to the vacuum level work function of a material [53]:

$$\Phi = E_{vac} - E_F \tag{3}$$

where E_{vac} is the vacuum energy level where an electron is positioned at rest outside of the material (free), and E_F is the Fermi energy level of a material, the observed change in work function clearly agrees with the Fermi energy level shift exhibited in Figure 3(c). Therefore, due to the direct relation of work function and E_F, the change in work function via annealing temperature can be said to be primarily owed to an increased extinction of carriers as annealing temperature rises.

The work function values of the films under current study are comparable to, while slightly greater than, the work functions of previously investigated heavily-doped AZO films (~4.7-5.2 eV)[24, 54]. These slight differences in work function can be attributed to differences in fabrication techniques and parameters, such as chamber pressure and/or deposition power that may cause differences in doping level and film surface sensitivity during photo-excitation. However, it is the significant shift in work function (up to ~0.5 eV) due to varied annealing temperatures that is of particular interest, providing an alternate method for the tuning of AZO's work function value. As mentioned previously, the ability to control the work function of a TCO film is of great importance when aiming to achieve Ohmic contact between the active/channel and electrode materials in an electronic device due to the enhanced charge transfer between layers [27, 55]. Non-Ohmic contact may occur due to mismatched work functions of the separate layers, known as a Schottky-like barrier, resulting in an increase of charge obstruction and ultimately limiting the charge transfer between layers [27, 55]. Thus, as stated prior, obtaining the ability to tune the work function of electrode materials is widely sought after, as mitigating the differences in work function between the channel and electrode layers allows for greater potential to achieve interfacial Ohmic contact. The trend exhibited in Figure 4(c) shows substantial promise as it provides a relatively simple method to tune the work function of AZO through post-fabrication air annealing. In comparison to the previously mentioned methods for tuning AZO at a fixed Al wt. % such as UV-ozone treatment (~0.4 eV shift) and acetone solvent cleaning (~0.1 eV shift)[34, 35], post-fabrication air-annealing exhibits a substantial shift of ~0.5 eV when annealed at 600 °C, indicating strong potential for the use of post-fabrication air-annealing as a viable work function tuning method for AZO.

To further verify that the change in work function of the AZO films is due to the carrier density reducing effects of post-fabrication air-annealing, XPS survey and core-level high resolution measurements were performed with the intent of determining the surface chemistry of major elements (i.e., Zn, O, Al). In Figure 5, the full XPS survey spectra (0 to 1350 eV) of the as-deposited and air-annealed AZO films can be observed. Survey spectra analysis reveals no significant differences between most of the AZO films; furthermore, all films clearly exhibit considerable peak intensities from the expected major elements of Zn, O, and Al. Prior to detailed analysis, it should be noted that the small peak located at 290 eV is owed to carbon contamination, possibly introduced during sample preparation or during the deposition process. Core-level high resolution XPS spectra of these elements are shown in Figure 6.

Figure 6 displays the core-level high-resolution XPS of the AZO films' (a) O 1s, (b) Zn 2p, and (c) Al 2p peaks and their chemical state variations due to increased air-annealing temperatures. The core-level O 1s spectra show asymmetry with two peaks centered at 532.4±0.1 eV and 531.1±0.1 eV. Utilizing Gaussian fitting, these peaks were de-convoluted and, for sake of comparison, will be denoted as O_1 and O_2 peaks, respectively. The peak located at the higher binding energy, O_1, can be attributed to O^{2-} ions in the oxygen deficient regions within the ZnO matrix, indicating the presence of oxygen vacancies [56, 57]. The peak located at the lower binding energy, O_2, is characteristic of an oxygen-sufficient state and attributed to O^{2-} ions on the wurtzite structure of a hexagonal Zn^{2+} array, surrounded by either Zn atoms or substitutional Al atoms [56]. The relative changes in the low and high binding energy peaks due to increasing annealing temperatures reveal critical information regarding the degree of O-Zn bonding and the amount of oxygen vacancies in the thin film [56]. The as-deposited AZO films in Figure 6(a) can be seen to

exhibit a dominate O_1 peak and thus are said to be in an oxygen deficient state. However, as annealing temperature is raised from 25 °C to 600 °C, the O_1 peak decreases in intensity while the O_2 peak increases in intensity, further verifying that the increasing of annealing temperatures promotes the extinction oxygen vacancies. This XPS data is in good agreement with both the VB and work function analyses, which attribute their distinct shifts to changes in carrier concentration via oxygen vacancy elimination.

The Zn 2p spectra exhibits a doublet consisting of two peaks occurring at 1045.5±0.1 eV and 1022.1±0.1 eV and are characteristic of Zn $2p_{1/2}$ and Zn $2p_{3/2}$, respectively[58]. The doublet Zn peaks are a result of spin orbit splitting, which occurs for the p, d, and f orbitals [59, 60]. For both Zn peaks, no notable change is seen throughout the variation of annealing temperatures. In all AZO films, as-deposited and annealed, $2p_{3/2}$ peaks are observed to be highly symmetric, occurring at 1022.1±0.1 eV. This value is less than that of bulk ZnO peaks which occur at 1022.4 eV, indicating that the majority of Zn atoms in the AZO films remains in the oxygen deficient Zn^{2+} valence state in the ZnO matrix [61, 62]. Furthermore, no metallic Zn peak could be observed at 1021.5 eV[62].

The Al 2p spectra exhibits a symmetric peak at a binding energy of 74.7±0.1 eV for all films. This peak is characteristic of aluminum oxide [1-2], indicating that the Al material present in the AZO films is bonded to oxygen in the form of Al_2O_3. No metallic peak was observed at 72.7±0.1 eV [56, 57], which indicates that the Al substitution of Zn in the wurtzite crystal structure went unobstructed and thus was not segregated as unreacted Al metal in the AZO films.

The transition of the AZO films from an oxygen-deficient to an oxygen-sufficient state was further analyzed via elemental composition ratios, displayed in Figure 7. To provide a better understanding of the varying chemical states of the AZO films, the ratio of oxygen content to the present cation species (Zn and Al) and the ratio of O_1 and O_2 peaks can be seen in Figures 7(a) and 7(b), respectively. The ratio of oxygen to cations were plotted as a function of inverse absolute temperature on an Arrhenius plot in Figure 7 (a) in order to obtain the activation energy of oxygen association/dissociation in the AZO films, which was found to be 33.3 meV. This is in good agreement with other activation energies found for oxygen vacancy annihilation in AZO films at similar annealing temperatures (32.6-91 meV) [63, 64] while also closely matching the activation energies for oxygen vacancy annihilation in ZnO films (20.0 meV) [65]. The relatively low activation energy for changes in carrier concentration can be justified due to the fact that the donor level of native defect dopants (oxygen vacancies) is located in a shallow energy level within the bandgap (0.5-1.2 eV below the conduction band) [66-68]. Due to the close proximity to the conduction band, a low thermal activation energy is required to significantly reduce (or generate) the amount of oxygen vacancies in AZO films. This aligns well with the low activation energy derived as well as with the significant transition from oxygen-deficiency to oxygen sufficiency at relatively low annealing temperatures.

To properly quantify the change in oxygen sufficient and deficient states, the ratio of the previously de-convoluted O_1 peak to the O_2 peak was plotted against annealing temperature in Figure 7(b). As the O_1:O_2 ratio decreases, a higher oxygen sufficient state is achieved due to a reduction of oxygen vacancies. The shift from an oxygen deficiency to a more oxygen sufficient state starts

rapidly from room temperature to 150 °C, but shifted much less drastically after 150°C, which is in accordance with the previously derived low activation energy of oxygen association/dissociation.

In order to analyze the effect of post-fabrication annealing on the optical properties of AZO, optical transmission measurements were gathered via UV-Vis spectroscopy. Figure 8(a) displays the transmission spectra for all AZO thin films over the wavelength range of 200-1000 nm. The average optical transmittance exhibited in the visible regime is >90% for all AZO films. The films also exhibit sharp fundamental optical absorption edges near ~385 nm, where light energy is absorbed due to the excitation of an electron from the valence band to the conduction band [69]. With annealing temperatures increasing from 100 °C to 600 °C, compared to as-deposited spectra, a clear red-shift of the UV absorption edge can be observed in Figure 8(a), indicating a narrowing in the optical band gap of the material (E_G). The shifting of the absorption edge to a greater wavelength region is known as the Burstein-Moss (BM) shift, which states that an increase in E_G is the result of an increase in carrier density due to the excess filling of electrons in the conduction band [70]. This relationship is defined via the BM equation:

$$\Delta E_G = \left(\frac{h^2}{8m^*}\right)\left(\frac{3n}{\pi}\right)^{2/3} \quad (4)$$

where m^* is the reduced effective mass of the election, n is the carrier concentration, h is Planck's constant, and ΔE_G is the change in optical band gap. As discussed prior, the excess formation of Zn interstitial atoms is unfeasible in this particular study and, thus, it can be firmly stated that the variations in carrier concentration and optical band gap of the AZO films are due primarily to the overall decrease in oxygen vacancies. Utilizing the transmission spectra measurements to further verify this trend, Figure 8(b) displays the square of the absorption coefficients, α, as a function of photon energy. As ZnO is known to be a direct semiconducting material [71], E_G values were

estimated via an extrapolation of the linear regime of α^2 vs. hv, which can be observed in Figure 8(c). As annealing temperature increases from 25 °C (as-deposited) to 600 °C, the optical band of AZO decreases from ~3.55 eV to 3.37 eV, respectively. According to the BM shift, the optical band gap shift can be directly explained due to the change in carrier concentration, which is in agreement with previously discussed XPS analysis of increased oxygen vacancy elimination due to heightened annealing temperatures and also with typical degenerated semiconducting materials such as IZO, ITO, and ZnO [72]. Furthermore, in comparison to prior studies of the optical band gaps in AZO thin films (2 wt. % Al_2O_3) and their response to increased annealing temperatures, deposited via both sol-gel techniques (~3.28 eV) and RF/DC magnetron sputtering (~3.3-3.6 eV), the E_G values of the DC magnetron sputtered AZO films in this study agree with established AZO band gap values and characteristics [73, 74].

4. Conclusion

In conclusion, this study has demonstrated a simple yet effective way to tune the band gap and work function of AZO films via post-fabrication air-annealing. A notable work function shift of ~0.5 eV was achieved at an annealing temperature of 600 °C, observed to be due to oxygen vacancy elimination. The increase in air-annealing temperature promotes oxygen in the air to fill native oxygen vacancies within the film, resulting in an overall decrease in carrier concentration and a Fermi shift towards the valence band. This theory was confirmed through XPS core-level high resolution analysis, where a distinct shift from an oxygen deficient- to an oxygen sufficient-state was observed in the O 1s peaks with increasing annealing temperature. For further verification of this trend, UV-vis spectroscopic analysis of the AZO films exhibited a decrease in the optical band gap (~3.55 eV to ~3.37 eV) with increased annealing temperatures (25°C (as-

deposited) to 600°C), suggesting a decrease in carrier density due to the Burstein-Moss relationship. Possessing the ability to tune the work function of AZO through straightforward post-fabrication air-annealing should provide an uncomplicated route for improved work function matching between AZO electrodes and various channel/active layer materials in novel electronic and optoelectronic devices.

Acknowledgements

The authors gratefully acknowledge the financial support from Purdue University and NSF grant, Award No. ECCS-1808168.

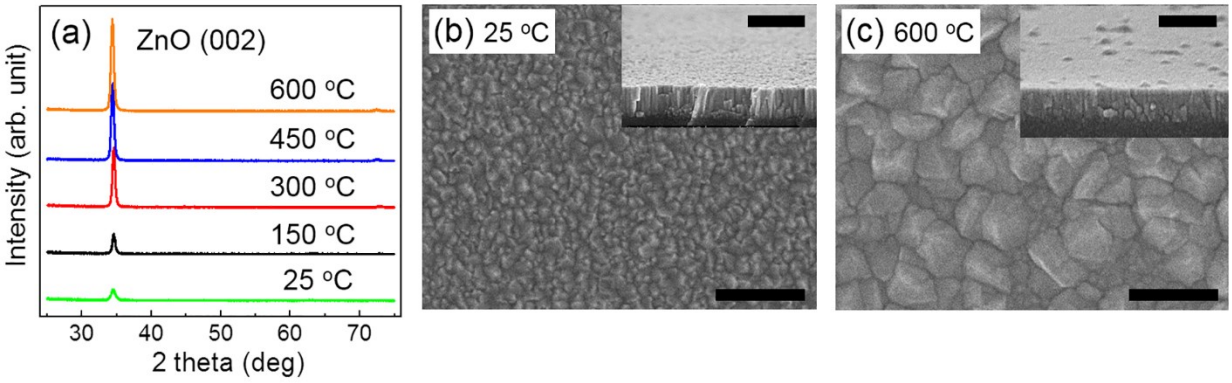

Figure 1. (a) X-Ray Diffraction data of ZnO thin film annealed at various temperatures: ZnO(002) shows enhanced intensity peak at the high temperature in annealing process. SEM images of ZnO thin film annealed (b) at room temperature (c) at 600°C. The inset of the images represent the cross-sectional view of the thin film. The scale bars represent 200 nm.

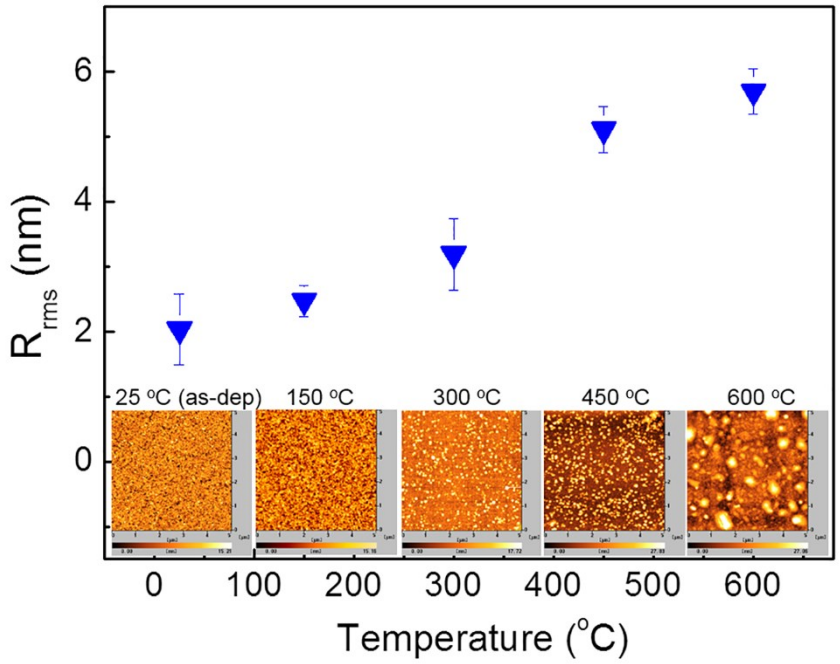

Figure 2. Atomic Force Microscope Images and RMS roughness values of the AZO films were taken at varying annealing temperatures to investigate the effect of air-annealing on the surface morphology of the films

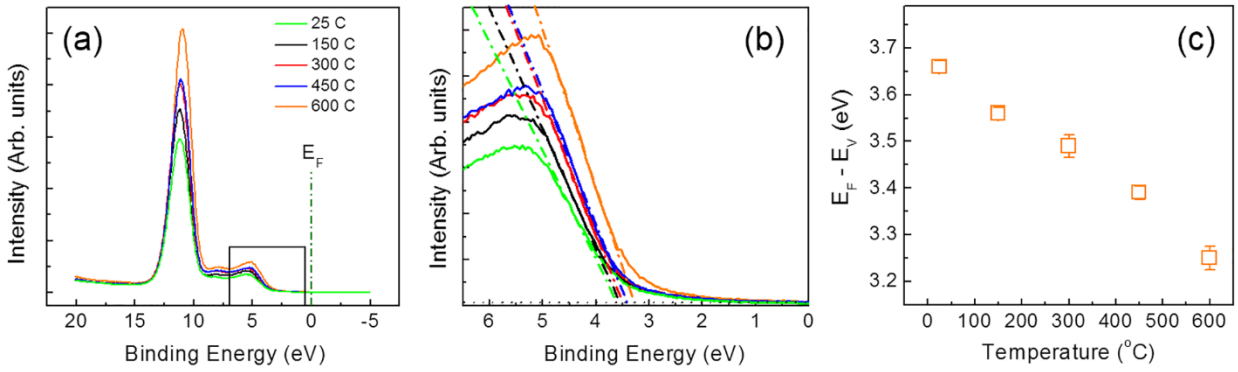

Figure 3. Utilizing XPS measurements, the Fermi-shifting effects of varying post-fabrication annealing temperatures on AZO thin films were found via observation of the (a,b) valence band spectra and (c) the Fermi band's relation to the valence band throughout separate annealing conditions (E_F - E_V).

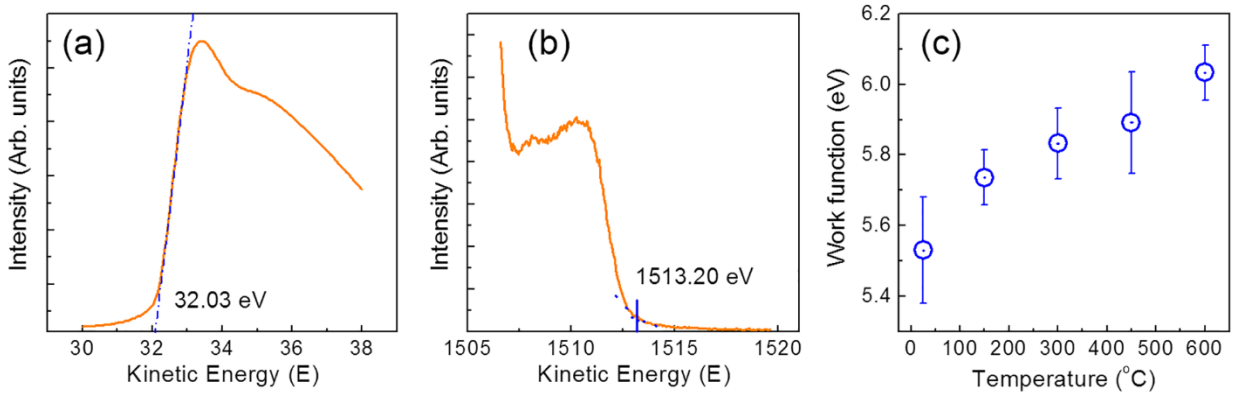

Figure 4. Utilizing XPS data, the work function values of all AZO samples were gathered by finding both the (a) secondary electron cut-off points (25 °C displayed) and the (b) high energy cut-off points (25 °C displayed). The (c) work function values obtained are then compared to their respective annealing temperatures.

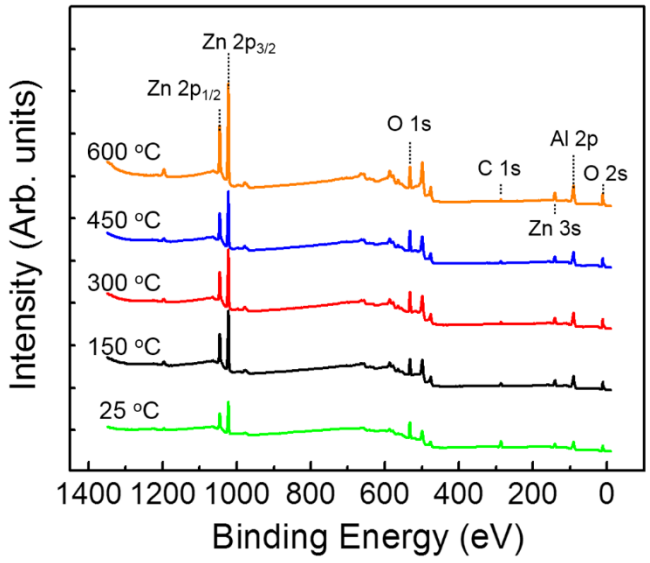

Figure 5. Full XPS Survey Scans of AZO films as deposited and annealed at 150 °C, 300 °C, 450 °C, and 600 °C. All films show characteristic peaks of Zn, O, Al, and C. Changes in these peaks were investigated to see the effect of annealing on the chemistry of the films.

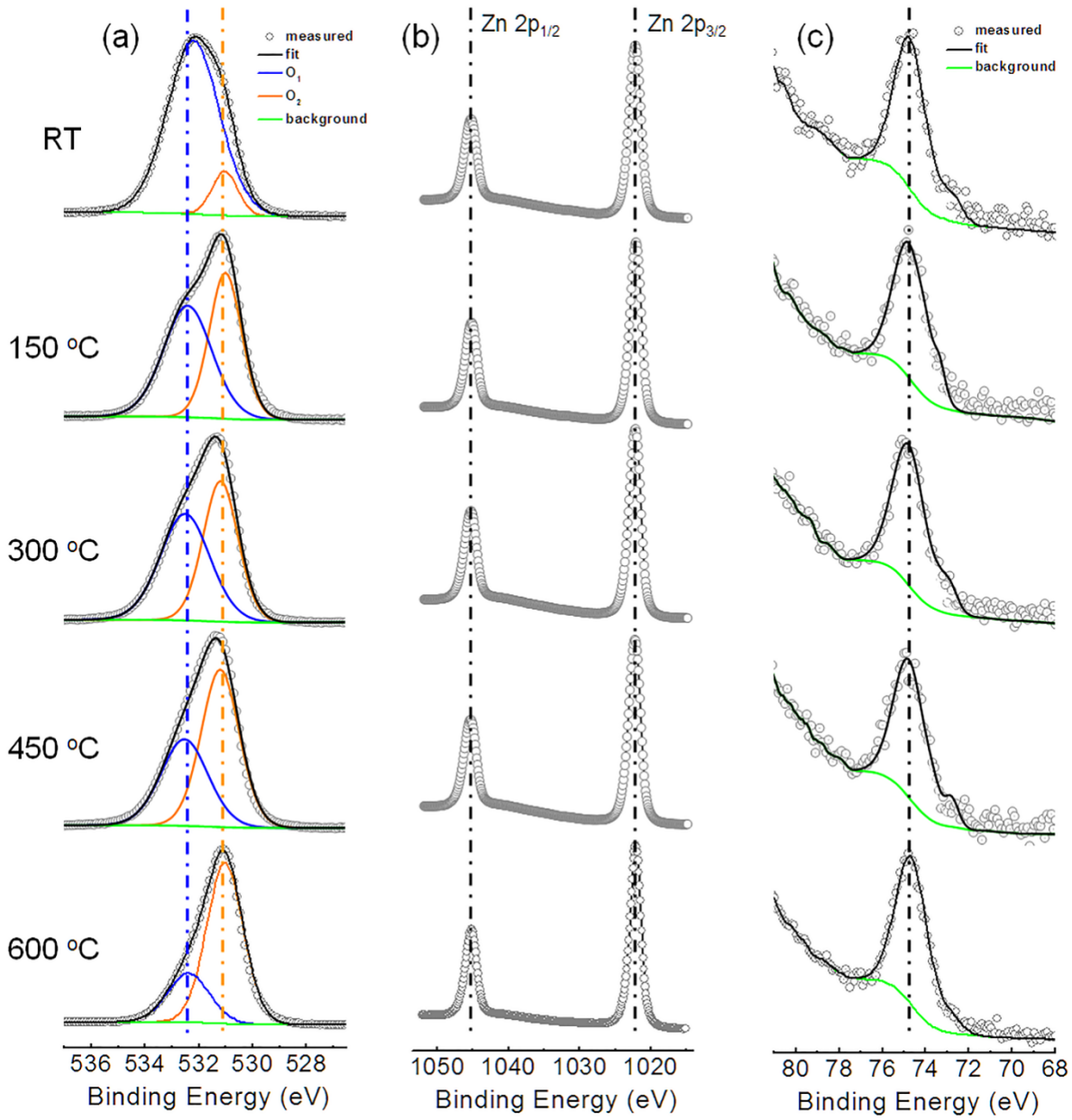

Figure 6. Core level high resolution XPS Spectra. (a) Asymmetric Oxygen 1s peak de-convoluted into O_1 and O_2, which are representative of oxygen deficient and sufficient states, respectively. (b) Zn 2p doublet which consists of a higher binding energy $2p_{1/2}$ and a lower binding energy $2p_{3/2}$ peak. (c) Aluminum 2p peak seen to be centered at a consistent binding energy with varying annealing temperature.

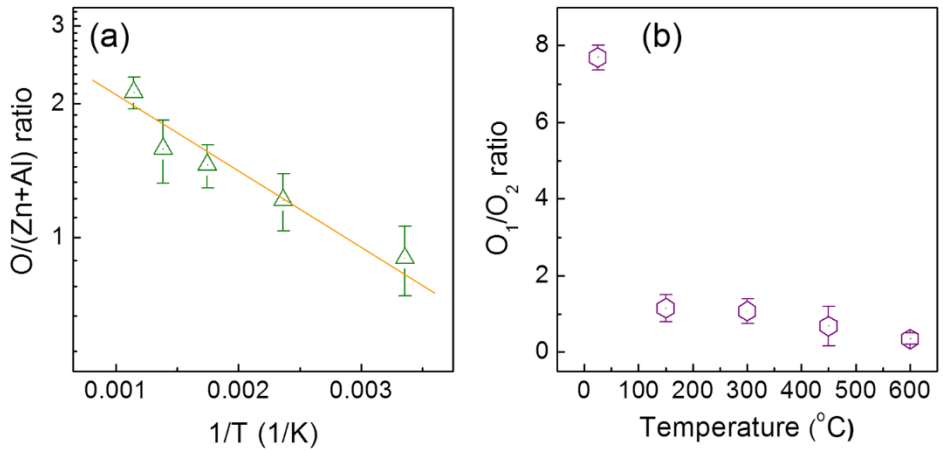

Figure 7. (a) Arrhenius plot of the ratio of oxygen content to that of Zn and Al cation species.(b) The ratio of the deconvoluted O_1 to the O_2 at varying annealing temperatures. These peaks are representative of an oxygen deficient state and an oxygen sufficient state, respectively.

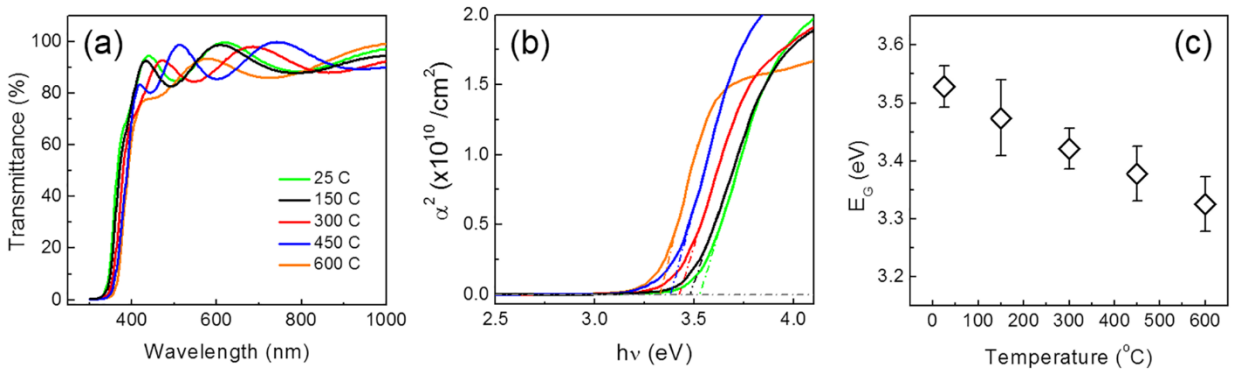

Figure 8. Effects of varying post-fabrication annealing temperatures on the (a) transmission and (b,c) optical bandgap values of AZO thin films.

References

[1] D.S. Ginley, C. Bright, Transparent conducting oxides, MRS bulletin 25(8) (2000) 15-18.
[2] B.G. Lewis, D.C. Paine, Applications and Processing of Transparent Conducting Oxides, MRS Bulletin 25(8) (2000) 22-27.
[3] S. Lee, H. Park, D.C. Paine, A study of the specific contact resistance and channel resistivity of amorphous IZO thin film transistors with IZO source-drain metallization, Journal of Applied Physics 109(6) (2011) 063702.
[4] J. Cui, A. Wang, N.L. Edleman, J. Ni, P. Lee, N.R. Armstrong, T.J. Marks, Indium Tin Oxide Alternatives—High Work Function Transparent Conducting Oxides as Anodes for Organic Light-Emitting Diodes, Advanced materials 13(19) (2001) 1476-1480.
[5] H. Kim, A. Piqué, J.S. Horwitz, H. Murata, Z.H. Kafafi, C.M. Gilmore, D.B. Chrisey, Effect of aluminum doping on zinc oxide thin films grown by pulsed laser deposition for organic light-emitting devices, Thin Solid Films 377-378 (2000) 798-802.
[6] R.G. Gordon, Criteria for Choosing Transparent Conductors, MRS Bulletin 25(8) (2000) 52-57.
[7] M. Chen, X. Wang, Y.H. Yu, Z.L. Pei, X.D. Bai, C. Sun, R.F. Huang, L.S. Wen, X-ray photoelectron spectroscopy and auger electron spectroscopy studies of Al-doped ZnO films, Applied Surface Science 158(1) (2000) 134-140.
[8] Y.-S. Kim, W.-P. Tai, Electrical and optical properties of Al-doped ZnO thin films by sol–gel process, Applied Surface Science 253(11) (2007) 4911-4916.
[9] T. Ratana, P. Amornpitoksuk, T. Ratana, S. Suwanboon, The wide band gap of highly oriented nanocrystalline Al doped ZnO thin films from sol–gel dip coating, Journal of Alloys and Compounds 470(1) (2009) 408-412.
[10] S.D. Bukkitgar, N.P. Shetti, R.M. Kulkarni, S.T. Nandibewoor, Electro-sensing base for mefenamic acid on a 5% barium-doped zinc oxide nanoparticle modified electrode and its analytical application, RSC Advances 5(127) (2015) 104891-104899.
[11] M. Tadatsugu, S. Hirotoshi, N. Hidehito, T. Shinzo, Group III Impurity Doped Zinc Oxide Thin Films Prepared by RF Magnetron Sputtering, Japanese Journal of Applied Physics 24(10A) (1985) L781.
[12] M. Tadatsugu, N. Hidehito, T. Shinzo, Highly Conductive and Transparent Aluminum Doped Zinc Oxide Thin Films Prepared by RF Magnetron Sputtering, Japanese Journal of Applied Physics 23(5A) (1984) L280.
[13] J. Hong, H. Paik, H. Hwang, S. Lee, A.J. deMello, K. No, The effect of growth temperature on physical properties of heavily doped ZnO:Al films, Physica Status Solidi a-Applications and Materials Science 206(4) (2009) 697-703.
[14] G.K. Paul, S.K. Sen, Sol–gel preparation, characterization and studies on electrical and thermoelectrical properties of gallium doped zinc oxide films, Materials Letters 57(3) (2002) 742-746.
[15] A. Sarkar, S. Ghosh, S. Chaudhuri, A.K. Pal, Studies on electron transport properties and the Burstein-Moss shift in indium-doped ZnO films, Thin Solid Films 204(2) (1991) 255-264.
[16] X. Jiang, F.L. Wong, M.K. Fung, S.T. Lee, Aluminum-doped zinc oxide films as transparent conductive electrode for organic light-emitting devices, Applied Physics Letters 83(9) (2003) 1875-1877.
[17] M. Hiramatsu, K. Imaeda, N. Horio, M. Nawata, Transparent conducting ZnO thin films prepared by XeCl excimer laser ablation, Journal of Vacuum Science & Technology A: Vacuum, Surfaces, and Films 16(2) (1998) 669-673.
[18] T.L. Yang, D.H. Zhang, J. Ma, H.L. Ma, Y. Chen, Transparent conducting ZnO:Al films deposited on organic substrates deposited by r.f. magnetron-sputtering, Thin Solid Films 326(1) (1998) 60-62.
[19] S. Lee, S.-H. Kim, Y. Kim, A.I. Kingon, D.C. Paine, K. No, Structural and electrical properties of transparent conducting Al2O3-doped ZnO thin films using off-axis DC magnetron sputtering, Materials Letters 85(0) (2012) 88-90.

[20] Z. Xiao, F. Guojia, W. Jiawei, L. Nishuang, L. Hao, W. Haolin, Z. Xingzhong, Enhanced performance of a -IGZO thin-film transistors by forming AZO/IGZO heterojunction source/drain contacts, Semiconductor Science and Technology 26(5) (2011) 055003.
[21] S. Dongfang, H. Dedong, H. Fuqing, T. Yu, Z. Suoming, C. Yingying, W. Yi, L. Lifeng, Z. Xing, Z. Shengdong, Fabrication and characteristics of fully transparent Aluminum-doped zinc oxide thin-film transistors, 2013 IEEE International Conference of Electron Devices and Solid-state Circuits, 2013, pp. 1-2.
[22] S. Sutthana, N. Hongsith, S. Choopun, AZO/Ag/AZO multilayer films prepared by DC magnetron sputtering for dye-sensitized solar cell application, Current Applied Physics 10(3) (2010) 813-816.
[23] W.J. Jeong, S.K. Kim, G.C. Park, Preparation and characteristic of ZnO thin film with high and low resistivity for an application of solar cell, Thin Solid Films 506-507 (2006) 180-183.
[24] H. Kim, J.S. Horwitz, W.H. Kim, A.J. Mäkinen, Z.H. Kafafi, D.B. Chrisey, Doped ZnO thin films as anode materials for organic light-emitting diodes, Thin Solid Films 420-421 (2002) 539-543.
[25] K.-U. Ritzau, M. Bivour, S. Schröer, H. Steinkemper, P. Reinecke, F. Wagner, M. Hermle, TCO work function related transport losses at the a-Si:H/TCO-contact in SHJ solar cells, Solar Energy Materials and Solar Cells 131 (2014) 9-13.
[26] S. Lee, H. Park, D.C. Paine, The effect of metallization contact resistance on the measurement of the field effect mobility of long-channel unannealed amorphous In-Zn-O thin film transistors, Thin Solid Films 520(10) (2012) 3769-3773.
[27] S. Chen, J.R. Manders, S.-W. Tsang, F. So, Metal oxides for interface engineering in polymer solar cells, Journal of Materials Chemistry 22(46) (2012) 24202-24212.
[28] S. Lee, K. Park, D.C. Paine, Metallization strategies for In2O3-based amorphous oxide semiconductor materials, Journal of Materials Research 27(17) (2012) 2299-2308.
[29] A. Godoy, L. Cattin, L. Toumi, F.R. Díaz, M.A. del Valle, G.M. Soto, B. Kouskoussa, M. Morsli, K. Benchouk, A. Khelil, J.C. Bernède, Effects of the buffer layer inserted between the transparent conductive oxide anode and the organic electron donor, Solar Energy Materials and Solar Cells 94(4) (2010) 648-654.
[30] M.A. Baldo, S.R. Forrest, Interface-limited injection in amorphous organic semiconductors, Physical Review B 64(8) (2001) 085201.
[31] J.S. Kim, J.H. Park, J.H. Lee, J. Jo, D.-Y. Kim, K. Cho, Control of the electrode work function and active layer morphology via surface modification of indium tin oxide for high efficiency organic photovoltaics, Applied Physics Letters 91(11) (2007) 112111.
[32] M.G. Helander, Z.B. Wang, J. Qiu, M.T. Greiner, D.P. Puzzo, Z.W. Liu, Z.H. Lu, Chlorinated Indium Tin Oxide Electrodes with High Work Function for Organic Device Compatibility, Science 332(6032) (2011) 944-947.
[33] C. Ganzorig, K.-J. Kwak, K. Yagi, M. Fujihira, Fine tuning work function of indium tin oxide by surface molecular design: Enhanced hole injection in organic electroluminescent devices, Applied Physics Letters 79(2) (2001) 272-274.
[34] W. Wang, Q. Feng, K. Jiang, J. Huang, X. Zhang, W. Song, R. Tan, Dependence of aluminum-doped zinc oxide work function on surface cleaning method as studied by ultraviolet and X-ray photoelectron spectroscopies, Applied Surface Science 257(9) (2011) 3884-3887.
[35] Q. Feng, W. Wang, K. Jiang, J. Huang, Y. Zhang, W. Song, R. Tan, Effect of deposition condition and UV-ozone post-treatment on work function of DC magnetron sputtered AZO thin films, Journal of Materials Science: Materials in Electronics 23(1) (2012) 267-272.
[36] A.V. Singh, R.M. Mehra, A. Yoshida, A. Wakahara, Doping mechanism in aluminum doped zinc oxide films, Journal of Applied Physics 95(7) (2004) 3640-3643.
[37] S. Yasushi, A. Toru, O. Nobuto, S. Yuzo, Carrier Density Dependence of Optical Band Gap and Work Function in Sn-Doped In 2 O 3 Films, Applied Physics Express 3(6) (2010) 061101.
[38] D.E. Eastman, Photoelectric Work Functions of Transition, Rare-Earth, and Noble Metals, Physical Review B 2(1) (1970) 1-2.

[39] S.-H.K. Park, Y.E. Lee, Controlling preferred orientation of ZnO thin films by atomic layer deposition, Journal of materials science 39(6) (2004) 2195-2197.
[40] J. Sengupta, R.K. Sahoo, C.D. Mukherjee, Effect of annealing on the structural, topographical and optical properties of sol–gel derived ZnO and AZO thin films, Materials Letters 83 (2012) 84-87.
[41] Y. Caglar, S. Ilican, M. Caglar, F. Yakuphanoglu, J. Wu, K. Gao, P. Lu, D. Xue, Influence of heat treatment on the nanocrystalline structure of ZnO film deposited on p-Si, Journal of Alloys and Compounds 481(1) (2009) 885-889.
[42] S.-Y. Kuo, W.-C. Chen, F.-I. Lai, C.-P. Cheng, H.-C. Kuo, S.-C. Wang, W.-F. Hsieh, Effects of doping concentration and annealing temperature on properties of highly-oriented Al-doped ZnO films, Journal of Crystal Growth 287(1) (2006) 78-84.
[43] A.G. Joshi, S. Sahai, N. Gandhi, Y.G.R. Krishna, D. Haranath, Valence band and core-level analysis of highly luminescent ZnO nanocrystals for designing ultrafast optical sensors, Applied Physics Letters 96(12) (2010) 123102.
[44] H.-J. Freund, P. K. Ghosh: Introduction to Photoelectron Spectroscopy, Vol. 67 aus: Chemical Analysis: A Series of Monographs on Analytical Chemistry and its Applications, John Wiley + Sons Ltd., New York, Chichester, Brisbane, Toronto, Singapore 1983. 377 Seiten, Preis: £ 52.25, Berichte der Bunsengesellschaft für physikalische Chemie 88(2) (1984) 183-184.
[45] S. Evans, WORK FUNCTION MEASUREMENTS BY X-PE SPECTROSCOPY, AND THEIR RELEVANCE TO CALIBRATION OF X-PE SPECTRA, Chemical Physics Letters 23(1) (1973) 134-138.
[46] E.T. Yu, E.T. Croke, D.H. Chow, D.A. Collins, M.C. Phillips, T.C. McGill, J.O. McCaldin, R.H. Miles, MEASUREMENT OF THE VALENCE BAND OFFSET IN NOVEL HETEROJUNCTION SYSTEMS - SI GE (100) AND ALSB ZNTE (100), Journal of Vacuum Science & Technology B 8(4) (1990) 908-915.
[47] G. Fang, D. Li, B.-L. Yao, Fabrication and vacuum annealing of transparent conductive AZO thin films prepared by DC magnetron sputtering, Vacuum 68(4) (2002) 363-372.
[48] S. Lee, D.C. Paine, Identification of the native defect doping mechanism in amorphous indium zinc oxide thin films studied using ultra high pressure oxidation, Applied Physics Letters 102(5) (2013) 052101.
[49] S. Lee, X. Guan, S. Ramanathan, Thin Film Oxy-Apatite Anodes for Solid Oxide Fuel Cells, J. Electrochem. Soc. 163(7) (2016) F719-F727.
[50] L.S. Debernardez, J. Ferron, E.C. Goldberg, R.H. Buitrago, THE EFFECT OF SURFACE-ROUGHNESS ON XPS AND AES, Surface Science 139(2-3) (1984) 541-548.
[51] P.L.J. Gunter, O.L.J. Gijzeman, J.W. Niemantsverdriet, Surface roughness effects in quantitative XPS: magic angle for determining overlayer thickness, Applied Surface Science 115(4) (1997) 342-346.
[52] C.R. Brundle, A.D. Baker, Electron Spectroscopy: Theory, Techniques, and Applications, Academic Press1978.
[53] A. Kahn, Fermi level, work function and vacuum level, Materials Horizons 3(1) (2016) 7-10.
[54] J. Zhao, S. Xie, S. Han, Z. Yang, L. Ye, T. Yang, Organic light-emitting diodes with AZO films as electrodes, Synthetic Metals 114(3) (2000) 251-254.
[55] L. Cattin, F. Dahou, Y. Lare, M. Morsli, R. Tricot, S. Houari, A. Mokrani, K. Jondo, A. Khelil, K. Napo, J.C. Bernède, MoO3 surface passivation of the transparent anode in organic solar cells using ultrathin films, Journal of Applied Physics 105(3) (2009) 034507.
[56] D.K. Kim, H.B. Kim, Room temperature deposition of Al-doped ZnO thin films on glass by RF magnetron sputtering under different Ar gas pressure, Journal of Alloys and Compounds 509(2) (2011) 421-425.
[57] H. Tong, Z. Deng, Z. Liu, C. Huang, J. Huang, H. Lan, C. Wang, Y. Cao, Effects of post-annealing on structural, optical and electrical properties of Al-doped ZnO thin films, Applied Surface Science 257(11) (2011) 4906-4911.

[58] S.K. Lim, S.H. Hong, S.-H. Hwang, W.M. Choi, S. Kim, H. Park, M.G. Jeong, Synthesis of Al-doped ZnO Nanorods via Microemulsion Method and Their Application as a CO Gas Sensor, Journal of Materials Science & Technology 31(6) (2015) 639-644.
[59] L.S. Wang, M.W. Xiao, X.J. Huang, Y.D. Wu, Synthesis, characterization, and photocatalytic activities of titanate nanotubes surface-decorated by zinc oxide nanoparticles, Journal of Hazardous Materials 161(1) (2009) 49-54.
[60] S.-S. Kim, J.-H. Yum, Y.-E. Sung, Flexible dye-sensitized solar cells using ZnO coated TiO2 nanoparticles, Journal of Photochemistry and Photobiology A: Chemistry 171(3) (2005) 269-273.
[61] M.N. Islam, T.B. Ghosh, K.L. Chopra, H.N. Acharya, XPS and X-ray diffraction studies of aluminum-doped zinc oxide transparent conducting films, Thin Solid Films 280(1) (1996) 20-25.
[62] W. Yang, Z. Liu, D.-L. Peng, F. Zhang, H. Huang, Y. Xie, Z. Wu, Room-temperature deposition of transparent conducting Al-doped ZnO films by RF magnetron sputtering method, Applied Surface Science 255(11) (2009) 5669-5673.
[63] K. Mohit, S.K. Hazra, S. Tapobrata, Role of metallic-like conductivity in unusual temperature-dependent transport in n-ZnO : Al/p-Si heterojunction diode, Journal of Physics D: Applied Physics 48(45) (2015) 455301.
[64] H. Noh Jun, I.S. Cho, S. Lee, M. Cho Chin, S. Han Hyun, J.S. An, H. Kwak Chae, Y. Kim Jin, S. Jung Hyun, J.K. Lee, S. Hong Kug, Photoluminescence and electrical properties of epitaxial Al-doped ZnO transparent conducting thin films, physica status solidi (a) 206(9) (2009) 2133-2138.
[65] Y. Yan, M.M. Al-Jassim, S.-H. Wei, Oxygen-vacancy mediated adsorption and reactions of molecular oxygen on the $\mathrm{ZnO}(10\overline{1}0)$ surface, Physical Review B 72(16) (2005) 161307.
[66] A. Janotti, C.G. Van de Walle, Oxygen vacancies in ZnO, Applied Physics Letters 87(12) (2005) 122102.
[67] S. Lany, A. Zunger, Anion vacancies as a source of persistent photoconductivity in II-VI and chalcopyrite semiconductors, Physical Review B 72(3) (2005) 035215.
[68] F. Oba, A. Togo, I. Tanaka, J. Paier, G. Kresse, Defect energetics in ZnO: A hybrid Hartree-Fock density functional study, Physical Review B 77(24) (2008) 245202.
[69] R.J. Collins, D.G. Thomas, Photoconduction and Surface Effects with Zinc Oxide Crystals, Physical Review 112(2) (1958) 388-395.
[70] E. Burstein, Anomalous Optical Absorption Limit in InSb, Physical Review 93(3) (1954) 632-633.
[71] M.D. McCluskey, S.J. Jokela, Defects in ZnO, Journal of Applied Physics 106(7) (2009) 071101.
[72] J.-W. Jeon, D.-W. Jeon, T. Sahoo, M. Kim, J.-H. Baek, J.L. Hoffman, N.S. Kim, I.-H. Lee, Effect of annealing temperature on optical band-gap of amorphous indium zinc oxide film, Journal of Alloys and Compounds 509(41) (2011) 10062-10065.
[73] J.G. Lu, S. Fujita, T. Kawaharamura, H. Nishinaka, Y. Kamada, T. Ohshima, Z.Z. Ye, Y.J. Zeng, Y.Z. Zhang, L.P. Zhu, H.P. He, B.H. Zhao, Carrier concentration dependence of band gap shift in n-type ZnO:Al films, Journal of Applied Physics 101(8) (2007) 083705.
[74] J.F. Chang, H.L. Wang, M.H. Hon, Studying of transparent conductive ZnO:Al thin films by RF reactive magnetron sputtering, Journal of Crystal Growth 211(1) (2000) 93-97.